PCCP

PAPER

View Article Online
View Journal | View Issue

Cite this: *Phys. Chem. Chem. Phys.*, 2025, **27**, 3997

First-principles elucidation of defect-mediated Li transport in hexagonal boron nitride†

Yilong Zhou, *[ab] S. O. Kucheyev[a] and Liwen F. Wan *[ab]

Received 21st September 2024,
Accepted 24th January 2025

DOI: 10.1039/d4cp03655g

rsc.li/pccp

Hexagonal boron nitride (hBN) is a promising candidate as a protective membrane or separator in Li-ion and Li–S batteries, given its excellent chemical stability, mechanical robustness, and high thermal conductivity. In addition, hBN can be functionalized by introducing defects and dopants, or be directly integrated into other active components of batteries, which further augments its appeal to the field. Here, we use first-principles simulations to evaluate the role of atomic defects in hBN in regulating the Li-ion diffusion mechanism and associated kinetics. Specifically, the following four distinct types of vacancy defects are considered: isolated single B and N vacancies, a B–N vacancy pair, and a B_3N vacancy cluster. It is found that these defect sites generally favor Li intercalation and out-of-plane diffusion but slow down in-plane Li-ion diffusion due to a strong Li trapping effect at the defect sites. Such a trapping effect is, however, highly local such that it does not necessarily affect the overall Li-ion conductivity in defected hBN layers. The present systematic evaluation of the impact of atomic defects on Li ion migration and accompanied charge analysis of hBN lattice in response to Li-ion diffusion provide a mechanistic understanding of Li-ion transport behavior in defected hBN and highlight the potential of defect engineering to achieve optimal material performance.

Despite continuous advances in materials formulation, interface engineering, and architecture design, fundamental challenges persist in rechargeable batteries for implementing Li metal as the optimal anode material and identifying and integrating a desired separator to prevent detrimental crossover shuttling events. These include transition metal dissolution in high-voltage Li batteries and polysulfide shuttling in Li–S batteries.[1–6] The major obstacle for implementing a Li metal anode is the formation of an unstable solid–electrolyte interface (SEI), which hinders Li-ion transport and charge transfer processes during repeated Li stripping and plating.[7,8] More importantly, the continuous growth of Li dendrites can short-circuit the electrochemical cell, leading to a catastrophic battery failure.[9–11] Various strategies have been proposed to improve interfacial stability and charge transport kinetics and to suppress the formation and growth of Li dendrites,[5,12,13] among which applying coatings has proven to be an effective approach. Hexagonal boron nitride (hBN), owing to its chemical inertness, mechanical robustness, and exceptional thermal conductivity,[14–22] could be an excellent choice as a coating material to enhance the thermal stability, alleviate SEI film cracking and suppress lithium dendrite growth in Li batteries[23–25] and effectively block polysulfide dissolution in Li–S batteries.[26]

Analogous to the structure of graphite, hBN is comprised of alternating layers of highly polarizable, sp^2-hybridized B and N. The layers are stacked together *via* weak van der Waals (vdW) forces.[17,18,22] As a result, pristine hBN is a wide bandgap insulator,[27,28] which has historically hindered its practicality as an electrode material in energy storage and conversion applications. However, hBN has found applications as components in composite separators or electrolytes and as protective or artificial SEI for electrode materials in rechargeable batteries.[23–26,29–31] For example, hBN-based composite separators in Li–S batteries can sufficiently block polysulfide migration, manage thermal distribution, and suppress dendrite growth.[26] Composite electrolytes based on hBN are also found effective to extend the working electrochemical window, warranting their application in next-generation high-voltage Li-ion batteries.[29,30] In addition, hBN has been used as a protective SEI in Li batteries to stabilize the Li anode, prevent dendrite growth, and enhance cycling stability.[31] Furthermore, significant headway has been made through various engineering approaches to extend hBN functionality.[32–35] For instance, hybridizing graphene oxide with hBN as a composite electrode material for Li-ion batteries can not only enhance thermal stability and increase the specific surface area of the

[a] *Materials Science Division, Lawrence Livermore National Laboratory, Livermore, California 94550, USA. E-mail: zhou17@llnl.gov, wan6@llnl.gov*
[b] *Laboratory for Energy Applications for the Future (LEAF), Lawrence Livermore National Laboratory, Livermore, California 94550, USA*

† Electronic supplementary information (ESI) available. See DOI: https://doi.org/10.1039/d4cp03655g

electrode—both of which are beneficial for its electrochemical performance—but also help to maintain the structural integrity of the anode during cycling, especially at elevated temperatures.[35]

Defect engineering has been demonstrated as an effective approach to tune materials properties. For instance, atomic defects can be readily introduced with a variety of synthetic or post-processing techniques.[36–41] In hBN, different types of vacancy defects, such as the isolated single B vacancy (V_B), single N vacancy (V_N), B–N pair vacancy (V_{BN}) and B_3N cluster vacancy (V_{B_3N}), have been commonly considered.[42,43] Vacancy defects can effectively alter the electronic and physicochemical properties of hBN for advanced applications.[44–46] When considering hBN as an active component in Li and Li–S batteries, a key question to address is the effect of lattice defects on Li-ion transport behavior in hBN. Most of previous work has been focused on the electronic properties of hBN,[43,47–49] with fewer explorations of its interaction with Li.[50,51]

Here, we carry out first-principles evaluation of the impact of four distinct atomic defects, V_B, V_N, V_{BN}, and V_{B_3N} (Fig. 1b), on Li-ion mobility in hBN. Both in-plane and out-of-plane Li-ion diffusion pathways (Fig. 1a) are considered. It is found that Li can be trapped at the defect sites due to local charge deficiency. However, once moving away from the defect sites, minimal impact is observed for in-plane Li-ion migration. In contrast, introducing these defects is found to have a major impact on out-of-plane Li-ion diffusion kinetics, where a significant decrease in activation energy is observed with increasing defect size. This finding is crucially important for the design and deployment of hBN as a separator or artificial SEI in next-generation high-performing Li batteries. Based on an exponential extrapolation of the activation energies of out-of-plane Li diffusion as a function of defect size, we speculate that defects with diameters larger than 4.4 Å, such as V_{BN}, would allow sufficient Li-ion transport (with a barrier <0.5 eV) through the hBN layers.

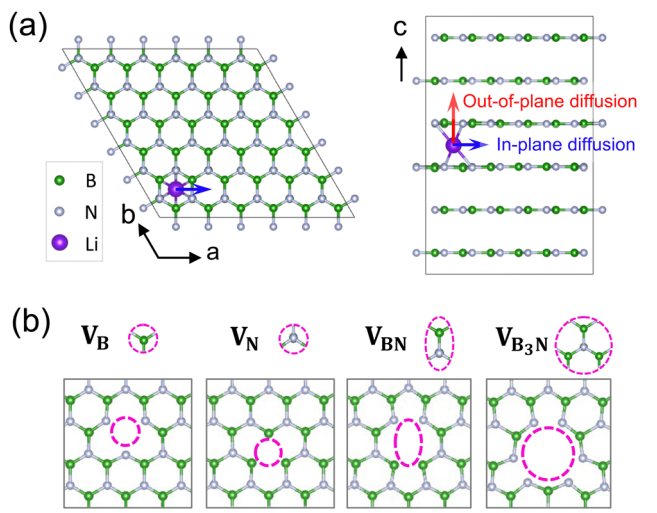

Fig. 1 Optimized structures of hBN, showing two distinct Li diffusion channels (a) and four types of vacancies (b) considered in the present study: single B vacancy (V_B), single N vacancy (V_N), BN pair vacancy (V_{BN}) and B_3N cluster vacancy (V_{B_3N}). The vacancy sites within the BN layer and their corresponding atomic configurations are highlighted by dashed circles in (b).

Followed by detailed calculations and discussion of Li-ion transport behavior in defected hBN, we first present reference results for Li-ion diffusion in pristine hBN. As depicted in Fig. 2a, three non-equivalent, high-symmetry atomic sites for Li insertion are identified: the hollow (H) site, between the centers of two hexagonal rings at adjacent layers; the tip (T) site, between the B and N atoms sitting across the alternating layers; and the edge (E) site, between the midpoints of the B–N bonds at two adjacent layers. These three distinct Li insertion sites are associated with three different local coordination environments of Li; *i.e.*, octahedral, tetrahedral, and linear with N atoms at the H, T and E site, respectively. The difference in local coordination environment effectively leads to variations in the Li intercalation energies as shown in Table S1 (ESI†). It is found that the thermodynamically most favorable potential intercalation site for Li is the H site, followed by E and T sites (also see Fig. S1, ESI†). The consistently positive intercalation energies obtained at these sites, regardless of the Li concentration (Fig. S2, ESI†), imply that minimal Li intercalation would be observed in pristine hBN.

Based on the layered geometry of hBN, two distinct Li-ion diffusion pathways are compared (Fig. 1a): in-plane diffusion, where Li migrates either within BN layers or between adjacent hBN layers, and out-of-plane diffusion, where Li passes across the hBN layers. Starting with Li at its thermodynamically most favorable intercalation site (H site), we calculate its diffusion barriers following two non-degenerated in-plane diffusion pathways, as shown in Fig. 2b. It is found that Li energetically prefers to migrate directly among the H sites, through the H–E–H pathway, as denoted in Fig. 2b, with an activation energy (E_a) of 0.34 eV. The slightly higher barrier observed along the H–T–E diffusion pathway (E_a = 0.4 eV) is due to the higher formation energy presented at the T site as shown in Table S1 (ESI†). Overall, these nudged elastic band (NEB) calculation results suggest sufficient Li-ion transport between the 2-dimensional BN layers. On the other hand, out-of-plane Li-ion diffusion, along the pathway depicted in Fig. 2c, would experience an extremely high barrier of 6.68 eV, implying impracticality of Li transport across the BN layers (also see Fig. S4, ESI†).

Intuitively, by introducing lattice defects, the hexagonal ring can be opened to permit Li-ion transport. Here, we compare effects of the following four types of hBN vacancies that are commonly discussed in the literature:[42,43] single B vacancy (V_B), single N vacancy (V_N), BN pair vacancy (V_{BN}) and B_3N cluster vacancy (V_{B_3N}) in a single layer of BN. The final relaxed structures of hBN containing these vacancies are presented in Fig. 1b. As expected, larger vacancies tend to be less stable as indicated by their formation energies shown in Table S2 (ESI†). The formation energies of V_B and V_N are found similar, which agree with previous work.[49] Considering these four types of vacancies, we evaluate their impact on Li intercalation energies. As shown in Fig. 3a, the introduction of these vacancies strongly modulates the local environment for Li intercalation. For example, Li is found energetically most favorable to reside

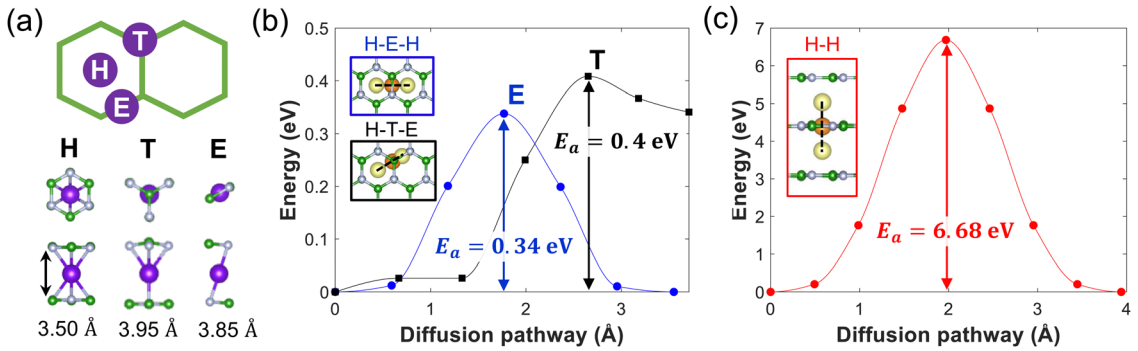

Fig. 2 Calculated Li-ion diffusion barriers in pristine hBN. (a) Schematic (top) and local atomic configurations of three high-symmetry Li intercalation sites, labeled H, T, and E. The middle and bottom frames in (a) depict the top and side views of Li position within the BN lattice. The changes of BN interlayer spacing upon Li incorporation at these different atomic sites are also highlighted. (b) and (c) Calculated energy profiles of Li migration along the in-plane (b) and out-of-plane (c) diffusion pathways. The associated activation energies are labeled as E_a, and the detailed Li migration pathways are rendered in the insets, where yellow spheres indicate the initial and final states, and brown spheres indicate the saddle points.

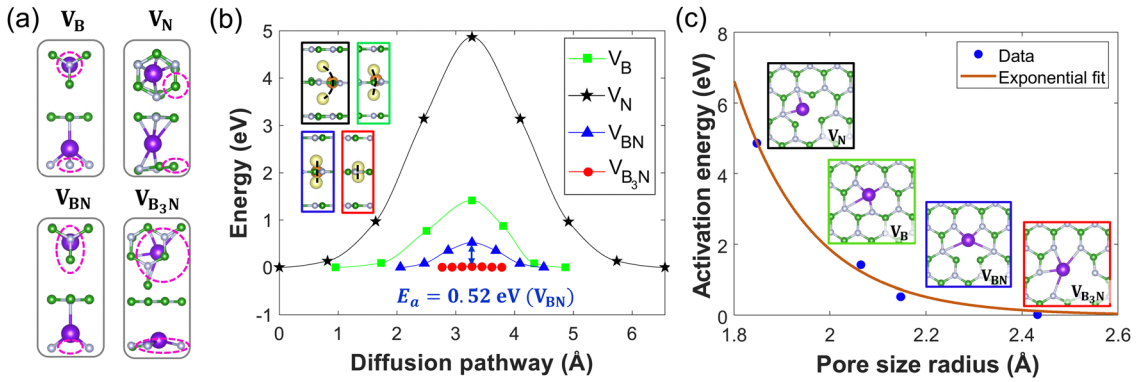

Fig. 3 Intercalation and out-of-plane diffusion of Li in defective hBN. (a) Top and side views illustrating Li intercalations at the preferred sites in the presence of vacancies. Dashed circles highlight vacancy positions. (b) Energy profiles of Li out-of-plane diffusion originating from the preferred intercalation sites shown in (a), with the associated Li migration pathways rendered in the insets (yellow spheres indicate the initial and final states, and brown spheres indicate the saddle points). (c) Activation energy as a function of pore size, with insets showing the geometries associated with saddle points in (b). The pore size radius is defined as the averaged distance of the Li from its six nearest neighboring atoms.

at the center just above the single B vacancy site (T site), while donating its extra valence electron to stabilize the surrounding charge deficient N atoms (Fig. S3a, ESI†). This charge compensation effectively results in a low Li intercalation energy of ~ -3 eV as shown in Table S3 (ESI†). In contrast, in the case of a single N vacancy, Li remains equidistant between the two BN layers but is off-centered from the vacancy. This positioning arises from its tendency to minimize unfavorable electrostatic interactions with the four positively charged B atoms surrounding the vacancy—three from the vacancy layer and one from the adjacent layer (Fig. S3b, ESI†). For the scenarios of larger vacancies, such as BN or B_3N, Li is attracted in closer proximity to the BN layer, similar to the case of a single B vacancy. Additionally, Li resides above the B vacant site in the case of a BN vacancy and between the two B vacant sites in the case of B_3N vacancy. It is interesting to note that charge transfer is generally observed from Li to its neighboring N atoms in the presence of B, BN, and B_3N vacancies, but the partial charges on the B atoms are largely unaffected (Fig. S3, ESI†). The enhanced electrostatic interactions resulting from this local charge redistribution effectively define favored Li intercalation energies at these defect sites, as shown in Table S3 (ESI†). In contrary, in the case of a N vacancy, charge transfer mainly occurs between Li and the two neighboring B atoms surrounding the vacancy while the charges on N atoms remain largely unaffected (Fig. S3b, ESI†), leading to unfavored Li incorporation (Table S3, ESI†).

We subsequently explore out-of-plane Li-ion diffusion from these intercalation sites (Fig. 3b and c). The distinct Li interaction with the single N vacancy, compared with other vacancies (*i.e.*, B, BN, and B_3N), also leads to its unique out-of-plane diffusion behavior. Unlike the cases of B, BN, and B_3N vacancies, Li migration through a single N vacancy follows a winding path (see the inset in Fig. 3b), passing through the saddle point, where Li forms two local bonds with surrounding N atoms (see the inset in Fig. 3c), necessitating a high activation energy of 4.87 eV. Conversely, with B, BN, or B_3N vacancies, Li migration follows almost straight paths through the vacancies (see insets

in Fig. 3b), forming four local bonds with surrounding N atoms at the saddle points (see insets in Fig. 3c). The favorable local atomic environment of Li at the saddle point effectively leads to lowered migration barriers. For example, in the case of a single B vacancy, the energy barrier drops to 1.42 eV. When fitting the migration barriers as a function of the pore size, it follows a nearly exponential decay, as shown in Fig. 3c. Specifically, defects with radii larger than 2.2 Å are expected to allow sufficient Li-ion transport with a barrier less than 0.5 eV. These observations, along with the charge density difference analyses (Fig. S4, ESI†), collectively support the notion that vacancies can effectively promote out-of-plane Li-ion diffusion, thereby converting hBN from a 2D to 3D Li-ion conductor for enhanced versatility.

Next, we examine in-plane Li-ion diffusion in defective hBN, starting with the case of a single B vacancy. Fig. 4a and Fig. S5a (ESI†) present the calculated in-plane Li-ion diffusion barriers along three distinct pathways, originated from the most stable Li intercalation site (T) highlighted in Fig. 3a. Following the same notations as in Fig. 2, the paths 1, 2, and 3 considered here echo Li-ion migration pathways of T–E–T–H–E–H, T–H–T–H–T–H, and T–H–T–H–T–H, respectively, in pristine hBN. As shown in Fig. 4a, a strong trapping effect is observed at the B vacancy site (also see Fig. S6, ESI†), where a high activation

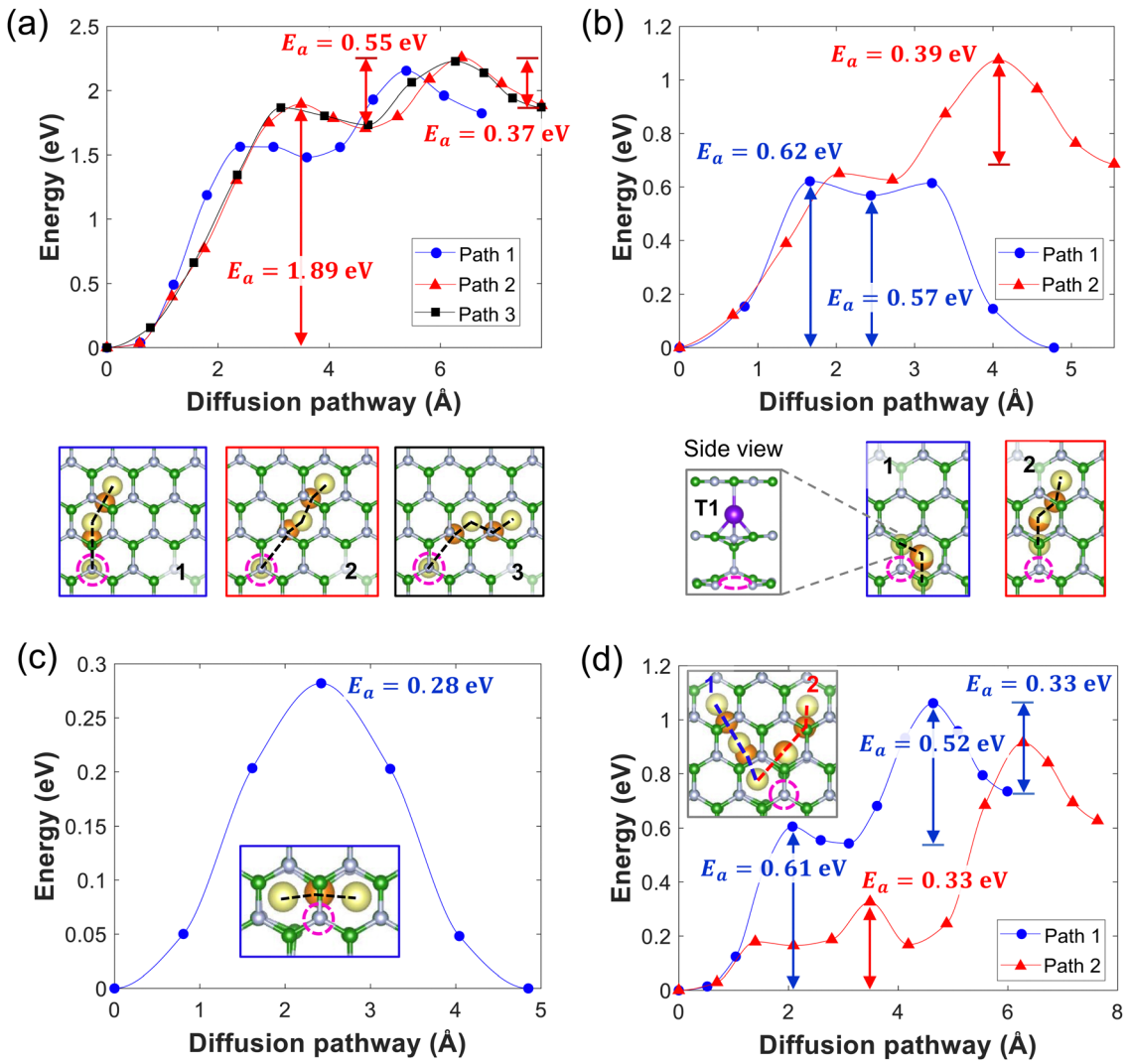

Fig. 4 In-plane diffusion of Li in hBN in the presence of B or N vacancies. (a) and (b) Energy profiles of Li migration in the presence of a B vacancy at the vacancy layer (a) along three distinct pathways: T–E–T–H–E–H (path 1), T–H–T–H–T–H (path 2), and T–H–T–H–T–H (path 3), and above the vacancy layer (b). The most stable intercalation site for the Li above the vacancy layer is identified as a T site (T1) adjacent to, rather than directly above (T0), the B vacancy (Table S4 and Fig. S7, ESI†). Li intercalation into the T1 site induces the formation of a BN bridge between two adjacent BN layers, where the B atom beneath the Li atom is pushed downward, and the N atom adjacent to the vacancy is pulled upward (side view in the inset). (c) and (d) Energy profile of Li migration in the presence of a N vacancy along a short H–T–H pathway adjacent to the vacancy (c) and along long diffusion pathways (d): H–E–H–E–H (path 1) and H–E–H–T–H (path 2). Associated activation energies (E_a) are labeled. Insets show the corresponding minimum energy diffusion pathways (yellow spheres indicate the initial, local-minimum, and final states; brown spheres indicate the saddle points), with the positions of vacancy highlighted by pink dashed circles. The activation energy of Li diffusion in pristine hBN is 0.34 eV.

energy of >1.5 eV is needed for Li to escape from the vacancy site. Even at the site above the defective BN layer, a noticeable trapping effect is evidenced (Fig. 4b) due to the strong electrostatic interactions between Li and the neighboring N atoms (Fig. S7, ESI†). These results are consistent with the formation energy calculation discussed above. As Li migrates away from the vacancy site (to a distance of ~5 Å within the defected layer and 3 Å in adjacent layers), its diffusion resembles the bulk behavior (Fig. S5b, ESI†). Notably, with one Li trapped at the B vacancy site (Fig. S8b, ESI†), the trapping effect is significantly reduced for an additional Li, where the activation energy is lowered to 0.45 eV for the second Li to escape the trapping site. This implies that the vacancy does not necessarily hinder the overall in-plane Li-ion conduction at high Li loading.

In the presence of a single N vacancy, Li-ion preferentially occupies the off-centered H site near the vacancy, as shown in Fig. 3a. Here, we explore in-plane Li-ion diffusion from this site. Fig. 4c reveals that Li-ion mobility around the vacancy site will not be strongly affected by the presence of the vacancy (also see path 2 in Fig. 4d), with a barrier of 0.28 eV compared to 0.34 eV of the pristine case (Fig. 2b). Note that for the single B vacancy case, no similar Li diffusion pathway (*i.e.*, around the vacancy site) is identified due to the more pronounced trapping effect (see Fig. S6, ESI†). For Li-ion migrating away from the vacancy site (path 1 in Fig. 4d), significantly higher activation barriers are observed. This again indicates strong trapping effects at defect sites although less pronounced compared to the single B vacancy case. As Li moves further away from the vacancy site (to a distance of 5 Å), its diffusion behavior resembles the bulk one (Fig. S5c, ESI†), similar to the case of a single B vacancy described above.

We further explored in-plane Li-ion diffusion in the presence of BN and B_3N vacancy clusters. Fig. S9 (ESI†) compares several in plane Li-ion diffusion pathways around the BN (Fig. S9a, ESI†) and B_3N (Fig. S9b, ESI†) vacancies and associated energetics. These pathways generally share energy profiles and feature characteristics akin to those observed in the case of a single B vacancy (Fig. 4a). A strong trapping effect, observed near the vacancy site, is alleviated at a distance of ~5–6 Å away from the vacancy. Additionally, the trapping effect is significantly reduced for a second Li when the vacancy is pre-filled with a Li (Fig. S8d, ESI†). Compared to smaller-size single vacancies, such as B, N, and B–N pair, larger vacancies, such as B_3N, seem to show longer-range impact on Li-ion diffusion (Fig. S9b, ESI†), which can be attributed to the higher degree of lattice distortion experienced in the presence of these larger defects.

The above results underscore the current need for a better understanding of the impact of lattice defects on Li-ion diffusion going beyond the simplest scenario of a single Li atom interacting with an isolated point defect. For example, exploring Li transport behavior at higher Li concentrations (Fig. S10, ESI†) and defect densities is equally intriguing and important to address the pivotal role of lattice defects in devising the overall Li-ion storage mechanism and transport kinetics.[52] Although this study primarily focuses on single vacancy defects, it would be interesting to extend this work to investigations of the impact of other defect types, such as interstitial atoms,[47] dislocations,[53] planar defects, and dopant atoms.[50] For example, previous studies have shown that substituting three N atoms of the hBN hexagonal ring with larger P atoms can substantially enhance the performance of BN sheets as anode materials in Na-ion batteries.[50] Furthermore, it is important for future research to evaluate the role of charged defects, introducing additional complex ion–electron interactions near or beyond the local defects sites and thereby altering Li-ion migration pathways and the associated energetics.

In summary, this study has investigated the influence of vacancy defects on Li intercalation and diffusion in hBN from first principles simulations. Four distinct vacancy defects (V_B, V_N, V_{BN}, and V_{B_3N}) have been systematically examined, and their impact on in-plane and out-of-plane Li-ion diffusion kinetics have been compared to that in the pristine hBN lattice. Our results have revealed that pristine hBN is predominately a 2D Li-ion conductor, with vastly different activation energies for in-plane and out-of-plane diffusion of 0.34 and 6.68 eV, respectively. The introduction of atomic vacancies, such as V_B, V_{BN}, and V_{B_3N}, is found effective to promote out-of-plane Li-ion diffusion, with negligible energy barriers for Li diffusion through larger defects with effective pore sizes of >2.2 Å in hBN layers. Although these atomic defects exhibit a strong trapping effect for in-plane Li-ion conduction, they do not necessarily slow down the overall Li-ion diffusion kinetics as the thermodynamic driving force for Li trapping is highly localized. For Li ions at distances >5 Å from a defect site, a negligible change of its diffusion behavior is observed. Moreover, in realistic diffusion conditions, with vacancy sites decorated by trapped Li atoms, their impact on additional in-plane Li-ion diffusion is less significant. Overall, introducing vacancies can transform hBN from a 2D into a 3D Li conductor by realizing out-of-plane Li-ion diffusion. This transformation holds great promise for applications such as separators or artificial SEI for advanced Li batteries. By tailoring the type and densities of defects in hBN, Li-ion transport kinetics can be significantly improved while simultaneously mitigating Li dendrite growth. These findings underscore the potential of defect engineering as a powerful strategy to optimize hBN's performance for a wide range of energy storage applications.

Data availability

The data supporting this article have been included as part of the ESI.†

Conflicts of interest

The authors declare that there are no conflicts of interest.

Acknowledgements

This work was performed under the auspices of the U.S. DOE by LLNL under Contract DE-AC52-07NA27344 and was supported by the LLNL-LDRD program under Project 22-ERD-049.

References

1 S. Martinet, Nanomaterials for rechargeable lithium batteries, *Nanomater. Sustainable Energy*, 2016, 471–512.
2 J.-M. Tarascon and M. Armand, Issues and challenges facing rechargeable lithium batteries, *Nature*, 2001, **414**(6861), 359–367.
3 D. Deng, Li-ion batteries: basics, progress, and challenges, *Energy Sci. Eng.*, 2015, **3**(5), 385–418.
4 J. B. Goodenough and Y. Kim, Challenges for rechargeable Li batteries, *Chem. Mater.*, 2010, **22**(3), 587–603.
5 H. Raza, S. Y. Bai, J. Y. Cheng, S. Majumder, H. Zhu and Q. Liu, *et al.*, Li–S Batteries: Challenges, Achievements and Opportunities, *Electrochem. Energy Rev.*, 2023, **6**, 1.
6 Y. V. Mikhaylik and J. R. Akridge, Polysulfide shuttle study in the Li/S battery system, *J. Electrochem. Soc.*, 2004, **151**(11), A1969–A1976.
7 J. Heine, P. Hilbig, X. Qi, P. Niehoff, M. Winter and P. Bieker, Fluoroethylene carbonate as electrolyte additive in tetraethylene glycol dimethyl ether based electrolytes for application in lithium ion and lithium metal batteries, *J. Electrochem. Soc.*, 2015, **162**(6), A1094.
8 A. Wang, S. Kadam, H. Li, S. Shi and Y. Qi, Review on modeling of the anode solid electrolyte interphase (SEI) for lithium-ion batteries, *NPJ Comput. Mater.*, 2018, **4**(1), 15.
9 F. Orsini, A. Du Pasquier, B. Beaudoin, J. Tarascon, M. Trentin and N. Langenhuizen, *et al.*, In situ scanning electron microscopy (SEM) observation of interfaces within plastic lithium batteries, *J. Power Sources*, 1998, **76**(1), 19–29.
10 B. Wu, Q. Liu, D. Mu, H. Xu, L. Wang and L. Shi, *et al.*, Suppression of lithium dendrite growth by introducing a low reduction potential complex cation in the electrolyte, *RSC Adv.*, 2016, **6**(57), 51738–51746.
11 A. Arya and A. L. Sharma, Electrolyte for energy storage/conversion (Li+, Na+, Mg2+) devices based on PVC and their associated polymer: a comprehensive review, *J. Solid State Electrochem.*, 2019, **23**(4), 997–1059.
12 W. S. Huang, X. N. Feng, X. B. Han, W. F. Zhang and F. C. Questions Jiang, and Answers Relating to Lithium-Ion Battery Safety Issues. Cell Reports Physical, *Science*, 2021, **2**, 1.
13 Y. Q. Chen, Y. Q. Kang, Y. Zhao, L. Wang, J. L. Liu and Y. X. Li, *et al.*, A review of lithium-ion battery safety concerns: The issues, strategies, and testing standards, *J. Energy Chem.*, 2021, **59**, 83–99.
14 S. Roy, X. Zhang, A. B. Puthirath, A. Meiyazhagan, S. Bhattacharyya and M. M. Rahman, *et al.*, Structure, Properties and Applications of Two-Dimensional Hexagonal Boron Nitride, *Adv. Mater.*, 2021, **33**(44), e2101589.
15 S. Angizi, S. A. A. Alem and A. Pakdel, Towards Integration of Two-Dimensional Hexagonal Boron Nitride (2D h-BN) in Energy Conversion and Storage Devices, *Energies*, 2022, **15**, 3.
16 D. Sun, Z. Sun, D. Yang, X. Jiang, J. Tang and X. Wang, Advances in boron nitride-based materials for electrochemical energy storage and conversion, *EcoEnergy*, 2023, **1**(2), 375–404.
17 R. Han, F. Liu, X. Wang, M. Huang, W. Li and Y. Yamauchi, *et al.*, Functionalised hexagonal boron nitride for energy conversion and storage, *J. Mater. Chem. A*, 2020, **8**(29), 14384–14399.
18 Q. Weng, X. Wang, X. Wang, Y. Bando and D. Golberg, Functionalized hexagonal boron nitride nanomaterials: emerging properties and applications, *Chem. Soc. Rev.*, 2016, **45**(14), 3989–4012.
19 S. Mateti, I. Sultana, Y. Chen, M. Kota and M. M. Rahman, Boron Nitride-Based Nanomaterials: Synthesis and Application in Rechargeable Batteries, *Batteries*, 2023, **9**(7), 344.
20 C. Sharma, P. Vanishree, B. Rani, N. Lohia, G. Swati and R. Srivastava, *et al.*, Electrochemical properties of two-dimensional hexagonal boron nitride nanosheets prepared by hydrothermal method, *Electrochim. Acta*, 2023, **463**, 142848.
21 N. Khossossi, D. Singh, W. Luo and R. Ahuja, Flexible 3D porous boron nitride interconnected network as a high-performance Li-and Na-ion battery electrodes, *Electrochim. Acta*, 2022, **421**, 140491.
22 J. Pu, K. Zhang, Z. Wang, C. Li, K. Zhu and Y. Yao, *et al.*, Synthesis and Modification of Boron Nitride Nanomaterials for Electrochemical Energy Storage: From Theory to Application, *Adv. Funct. Mater.*, 2021, **31**(48), 2106315.
23 B. Mortazavi, H. Yang, F. Mohebbi, G. Cuniberti and T. Rabczuk, Graphene or h-BN paraffin composite structures for the thermal management of Li-ion batteries: a multiscale investigation, *Appl. Energy*, 2017, **202**, 323–334.
24 M. Waqas, S. Ali, D. Chen, B. Boateng, Y. Han and M. Zhang, *et al.*, A robust bi-layer separator with Lewis acid-base interaction for high-rate capacity lithium-ion batteries, *Composites, Part B*, 2019, **177**, 107448.
25 M. Waqas, S. Ali, W. Lv, D. Chen, B. Boateng and W. He, High-performance PE-BN/PVDF-HFP bilayer separator for lithium-ion batteries, *Adv. Mater. Interfaces*, 2019, **6**(1), 1801330.
26 P. J. H. Kim, J. Seo, K. Fu, J. Choi, Z. Liu and J. Kwon, *et al.*, Synergistic protective effect of a BN-carbon separator for highly stable lithium sulfur batteries, *NPG Asia Mater.*, 2017, **9**(4), e375.
27 B. Arnaud, S. Lebègue, P. Rabiller and M. Alouani, Huge excitonic effects in layered hexagonal boron nitride, *Phys. Rev. Lett.*, 2006, **96**, 2.
28 C. E. Ekuma, V. Dobrosavljevic and D. Gunlycke, First-Principles-Based Method for Electron Localization: Application to Monolayer Hexagonal Boron Nitride, *Phys. Rev. Lett.*, 2017, **118**, 10.
29 M. T. F. Rodrigues, K. Kalaga, H. Gullapalli, G. Babu, A. L. M. Reddy and P. M. Ajayan, Hexagonal boron nitride-based electrolyte composite for Li-ion battery operation from room temperature to 150 C. Advanced Energy, *Materials*, 2016, **6**(12), 1600218.
30 J.-H. Kim, D.-H. Park, J.-S. Jang, J.-H. Shin, M.-C. Kim and S.-B. Kim, *et al.*, High-performance free-standing hybrid solid electrolyte membrane combined with Li6. 28Al0. 24La3Zr2O12 and hexagonal-BN for all-solid-state lithium-based batteries, *Chem. Eng. J.*, 2022, **446**, 137035.

31 T. Ma, R. Wang, S. Jin, S. Zheng, L. Li and J. Shi, *et al.*, Functionalized boron nitride-based modification layer as ion regulator toward stable lithium anode at high current densities, *ACS Appl. Mater. Interfaces*, 2021, **13**(1), 391–399.
32 C. Liu, C. Wang, X. Meng, X. Li, Q. Qing and X. Wang, *et al.*, Tungsten nitride nanoparticles anchored on porous boro-carbonitride as high-rate anode for lithium ion batteries, *Chem. Eng. J.*, 2020, **399**, 125705.
33 S. Chen, H. Yang, Q. Chen, L. Liu, X. Hou and L. Luo, *et al.*, Synthesis of BCN nanoribbons from coconut shells using as high-performance anode materials for lithium-ion batteries, *Electrochim. Acta*, 2020, **346**, 136239.
34 D. Jia, R. Tong, L. Ning, Z. Yang, Y. Zhang and W. Gu, *et al.*, BN nanosheets in-situ mosaic on MOF-5 derived porous carbon skeleton for high-performance lithium-ion batteries, *J. Alloys Compd.*, 2021, **857**, 157571.
35 Y. Mussa, F. Ahmed, M. Arsalan and E. Alsharaeh, Two dimensional (2D) reduced graphene oxide (RGO)/hexagonal boron nitride (h-BN) based nanocomposites as anodes for high temperature rechargeable lithium-ion batteries, *Sci. Rep.*, 2020, **10**(1), 1882.
36 X. Wei, M.-S. Wang, Y. Bando and D. Golberg, Electron-beam-induced substitutional carbon doping of boron nitride nanosheets, nanoribbons, and nanotubes, *ACS Nano*, 2011, **5**(4), 2916–2922.
37 T. T. Tran, C. Elbadawi, D. Totonjian, C. J. Lobo, G. Grosso and H. Moon, *et al.*, Robust multicolor single photon emission from point defects in hexagonal boron nitride, *ACS Nano*, 2016, **10**(8), 7331–7338.
38 G. Grosso, H. Moon, B. Lienhard, S. Ali, D. K. Efetov and M. M. Furchi, *et al.*, Tunable and high-purity room temperature single-photon emission from atomic defects in hexagonal boron nitride, *Nat. Commun.*, 2017, **8**(1), 1–8.
39 J. Comtet, E. Glushkov, V. Navikas, J. Feng, V. Babenko and S. Hofmann, *et al.*, Wide-field spectral super-resolution mapping of optically active defects in hexagonal boron nitride, *Nano Lett.*, 2019, **19**(4), 2516–2523.
40 K. S. Kim, M. Couillard, H. Shin, M. Plunkett, D. Ruth and C. T. Kingston, *et al.*, Role of hydrogen in high-yield growth of boron nitride nanotubes at atmospheric pressure by induction thermal plasma, *ACS Nano*, 2018, **12**(1), 884–893.
41 R. Sevak Singh, R. Yingjie Tay, W. Leong Chow, S. Hon Tsang, G. Mallick and E. H. Tong Teo, Band gap effects of hexagonal boron nitride using oxygen plasma, *Appl. Phys. Lett.*, 2014, **104**, 16.
42 Q. Wang, Q. Zhang, X. Zhao, X. Luo, C. P. Y. Wong and J. Wang, *et al.*, Photoluminescence upconversion by defects in hexagonal boron nitride, *Nano Lett.*, 2018, **18**(11), 6898–6905.
43 J. Zhang, R. Sun, D. Ruan, M. Zhang, Y. Li and K. Zhang, *et al.*, Point defects in two-dimensional hexagonal boron nitride: A perspective, *J. Appl. Phys.*, 2020, **128**, 10.
44 Q. Weng, G. Li, X. Feng, K. Nielsch, D. Golberg and O. G. Schmidt, Electronic and optical properties of 2D materials constructed from light atoms, *Adv. Mater.*, 2018, **30**(46), 1801600.
45 S. Radhakrishnan, D. Das, A. Samanta, C. A. de Los Reyes, L. Deng and L. B. Alemany, *et al.*, Fluorinated h-BN as a magnetic semiconductor, *Sci. Adv.*, 2017, **3**(7), e1700842.
46 Q. Weng, D. G. Kvashnin, X. Wang, O. Cretu, Y. Yang and M. Zhou, *et al.*, Tuning of the optical, electronic, and magnetic properties of boron nitride nanosheets with oxygen doping and functionalization, *Adv. Mater.*, 2017, **29**(28), 1700695.
47 J. Strand, L. Larcher and A. L. Shluger, Properties of intrinsic point defects and dimers in hexagonal boron nitride, *J. Phys.: Condens. Matter*, 2020, **32**(5), 055706.
48 L. Weston, D. Wickramaratne, M. Mackoit, A. Alkauskas and C. G. Van de Walle, Native point defects and impurities in hexagonal boron nitride, *Phys. Rev. B*, 2018, **97**, 21.
49 B. Huang and H. Lee, Defect and impurity properties of hexagonal boron nitride: A first-principles calculation, *Phys. Rev. B*, 2012, **86**, 24.
50 A. Hosseinian, S. Soleimani-amiri, S. Arshadi, E. Vessally and L. Edjlali, Boosting the adsorption performance of BN nanosheet as an anode of Na-ion batteries: DFT studies, *Phys. Lett. A*, 2017, **381**(24), 2010–2015.
51 S. Kansara, S. K. Gupta, Y. Sonvane, M. V. Pajtler and R. Ahuja, Inquisitive geometric sites in h-BN monolayer for alkali earth metal ion batteries. The, *J. Phys. Chem. C*, 2019, **123**(32), 19340–19346.
52 H. Yildirim, A. Kinaci, Z. J. Zhao, M. K. Chan and J. P. Greeley, First-principles analysis of defect-mediated Li adsorption on graphene, *ACS Appl. Mater. Interfaces*, 2014, **6**(23), 21141–21150.
53 O. Cretu, Y.-C. Lin and K. Suenaga, Evidence for active atomic defects in monolayer hexagonal boron nitride: a new mechanism of plasticity in two-dimensional materials, *Nano Lett.*, 2014, **14**(2), 1064–1068.